

Ultralarge Contraction Directed by Light-Driven Unlocking of Prestored Strain Energy in Linear Liquid Crystal Polymer Fibers

Xinlei Pang, Lang Qin, Bo Xu, Quan Liu, and Yanlei Yu*

Anisotropic 1D contraction motion of polymeric actuating materials has drawn growing interests in fields ranging from soft robotics to biomimetic muscles. Although light-driven liquid crystal polymers (LCPs) represent promising candidates to realize contraction (<20%) triggered remotely and spatially, there remain multitudes of challenges to develop an LCP system possessing ultralarge contraction rate. Here, a novel strategy combining shape memory effect and photochemical phase transition is presented to realize light-driven contraction as large as 81% in a newly designed linear liquid crystal copolymer, where the eutectic mesogens of azobenzene and phenyl benzoate self-organize into the smectic B phase. Importantly, this highly ordered structure as the switching segment firmly locks the stress-induced strain energy, which is rapidly released by reversible *trans*–*cis* photoisomerization that destroys the lamellar liquid crystal phase, therefore leading to such ultralarge contraction. Fibers serve as light-driven building blocks to achieve precise origami, to mimic the recovery of a “broken” spider web and to screen objects in different sizes, laying new ground for advanced applications of light-driven LCPs from biomimetic robots to human assists.

1. Introduction

Anisotropic contraction, notably 1D contraction, is an effective motion for living creatures in nature to develop a series of self-protection and/or survival strategies. For instance, spider dragline silks are able to contract up to 50% of their original length in response to high humidity, which enables the spider web to recover wind- or impact-induced damage simply by the morning dew forming on the web.^[1] For another example, mammalian skeletal muscles that are often simplified as line segments without accounting for the large muscle attachment areas can generate active forces by 1D contraction of muscle fibers during physical exercise.^[2] Inspired by biological species, scientists have made great efforts to fabricate actuators with contractile functionalities in response to external stimuli,


showing potential applications in the field of soft robotics, smart woven textiles, biomimetic muscles, etc.^[3]

Polymeric actuating materials have received widespread attention when research into stimuli-responsive materials afforded concepts and building blocks that proved to be useful in the context of 1D contraction.^[4] An ideal candidate to realize large, 1D contraction is the liquid crystal polymer (LCP) because the liquid crystal (LC) molecules could be oriented in an ordered state and transform into a disordered state induced by thermal (photo-thermal)^[5] or photochemical^[6] LC-isotropic phase transition that gives access to large contraction. Thermal-driven contraction has been widely investigated by heating crosslinked LCPs above the isotropic transition temperature (T_{iso}), in which mesogens lose their uniaxially ordered alignment obtained by external force^[5a,b,d-f,k,m] or alignment layer,^[5i,j] and consequently

disorganize into random orientation. For example, Naciri et al. developed the LC terpolymer fibers with two side-chain mesogens and a non-mesogenic group that acted as a reactive site for crosslinking, exhibiting thermal-driven contraction with a rate of 30–35%, which was defined as $f = ((l_0 - l')/l_0) \times 100\%$ (l_0 is the original length of the material and l' is the length after complete contraction).^[5f] Recently, Yang and co-workers reported an interpenetrating LC polyurethane/polyacrylate elastomer, whose stretched film showed a maximum contraction rate of 46% at 140 °C and maintained ultrastrong actuation-mechanic properties.^[5d]

The other mechanism of contraction in LCPs is photochemical phase transition based on both the isomerization of a photoswitch and cooperative effect in LCs. The well-known azobenzene groups have usually been incorporated into polymer networks as a molecular trigger, since rod-like *trans*-isomers stabilize LC phases whereas *cis*-isomers disturb molecular alignment.^[7] The accumulation of *cis*-isomers upon *trans*–*cis* photoisomerization reduces the T_{iso} of LCPs and results in order–disorder phase transition when the T_{iso} is below experimental temperature.^[8] Finkelmann et al. preceded in the synthesis of azobenzene-containing elastomeric networks with polysiloxanes as main chains and demonstrated a UV-light-driven contraction by 20% at room temperature.^[6a] Later on, Keller et al. reported a side-on acrylate-based crosslinked LCP

X. Pang, Dr. L. Qin, Dr. B. Xu, Dr. Q. Liu, Prof. Y. Yu
Department of Materials Science and State Key Laboratory
of Molecular Engineering of Polymers
Fudan University
Shanghai 200433, China
E-mail: ylyu@fudan.edu.cn

 The ORCID identification number(s) for the author(s) of this article can be found under <https://doi.org/10.1002/adfm.202002451>.

DOI: 10.1002/adfm.202002451

showing the light-driven contraction of 18% by heating the film to 70 °C to activate the chain mobility.^[6b] However, these approaches still suffer from intrinsic limitation in the insufficient molecular order change that results in a small contraction rate. Thus, it remains multitudes of challenges to realize large contraction rate in the development of actuation strategy and material design.

Following the principle of shape memory effect (SME), the large shape changes of polymers have been readily achieved due to changes of the conformational entropy.^[9] Typically, the shape fixing and recovery processes are accompanied with the storage and release of the strain energy, which is realized by the freezing and activation of the long-range motion of polymer chains under the cooperative effect of net points and switching segments.^[10] Inspired by the design of strain energy in SME enabling large shape changes, we hypothesize that this effect might be applied to achieve large contraction rate in LCPs.

Herein, we present a new strategy to realize light-driven contraction as large as 81% based on the storage and release of the strain energy in linear liquid crystal polymer (LLCP) fibers (Figure 1a). The basic idea for our design inherited from SME is to utilize LC phase as the switching segment to control the strain energy, which is locked by the highly ordered LC structure and unlocked by the order–disorder phase transition upon reversible *trans–cis* photoisomerization of azobenzene mesogens. We further demonstrated that these fibers acted as light-driven building blocks to achieve precise origami, to mimic the recovery of a “broken” spider web, and to screen objects in different sizes.

2. Results and Discussion

To realize the large contraction, we designed the molecular structure of an LCP based on two requirements: 1) the strain energy must be locked by LC phase, and 2) the prestored strain energy must be unlocked and released upon irradiation with light. To satisfy the first requirement, the highly ordered LC phase was considered as the essential switching segment to lock the strain energy. We expected the linear structure to enable the facile fabrication of fibers by stretching, as well as the flexible backbone and long spacer to provide enough free volume for mesogens to self-assemble into a lamellar structure to lock the strain energy.^[11] The azobenzene moiety was selected as both a mesogen and a photosensitive group to meet the second requirement, which underwent isomerization to induce the order–disorder phase transition and then unlock the prestored strain energy. To facilitate the release of strain energy, the commonly used phenyl benzoate group as the eutectic mesogen was introduced to reduce the glass transition temperature (T_g) and largely activated the chain mobility.^[12] The molecular structure and size of phenyl benzoate mesogens are similar to those of azobenzene mesogens, which are also beneficial for their coassembly into the same lamellar structure. From these principles, we synthesized a novel LLCP with azobenzene and phenyl benzoate side chains (Figure 1b; Figures S1–S3, Supporting Information). As expected, this LLCP displayed a T_g at 17 °C and was in a high-elastic state with activated chain mobility at room temperature (Figure S4, Supporting Information).

The ring-opening metathesis polymerization enabled the high number-average molecular weight of the LLCP reaching up to 3.0×10^5 g mol⁻¹ (Figure S5, Supporting Information), which ensured enough mechanical robustness for actuators.

The changes in LC phase during the fabrication of LLCP fibers are shown schematically in Figure 1c–f. The melted polymer was firstly stretched at 83 °C higher than T_{iso} , where the backbones were preferentially oriented along the stretching direction while the mesogens were still disordered in the isotropic phase (Figure 1c). Then, both ends of the fiber were fixed and cooled down to room temperature (Figure 1d). We note that the azobenzene and phenyl benzoate mesogens in side chains self-assembled into a lamellar structure when the fiber was cooled below T_{iso} , which is evidenced by the emergence of two diffraction peaks with q ratio of 1:2 in the low-angle region of the 1D small-angle X-ray scattering (1D SAXS) profiles (Figure 1g). As shown in the 2D X-ray diffraction (2D XRD) measurement carried out on a fiber (the stretching ratio is 900%) at 60 °C (Figure S6, Supporting Information), the diffuse arcs in the high-angle region located on the meridian and the diffractions located on the equator indicate the formation of smectic A (SmA) layer structure in which the direction of normal axis is perpendicular to the stretching direction. Upon cooling to room temperature, the fiber remained the fixed shape without a rebound (Figure 1e). The emerging of azimuthal distribution of diffraction arcs in the high-angle region suggests that the side-chain mesogens form into a highly ordered smectic B (SmB) phase to constrain the movement of backbones and lock the strain energy in the fiber (Figure 1h; Figure S7, Supporting Information),^[13] which is similar to the storage of the strain energy in SME.

It is important to note that the contraction of this fiber was triggered by 470 nm light as a “key” at room temperature (Figure 1f), which induced the order–disorder phase transition upon *trans–cis* isomerization of azobenzene mesogens (Figure S8, Supporting Information), activated the polymer-chain mobility for relaxation and unlocked the strain energy prestored in the backbones. Therefore, the light-driven contraction as large as 81% of the LLCP fiber was realized. The disappearance of diffraction arcs in the high-angle region and the weakness of diffraction points in the low-angle region indicate that the mesogens are disordered and the periodic layer structures are disrupted, which are confirmed by 2D XRD measurement (Figure 1i).

The macroscopic deformation of LCPs is coupled with the alignment of mesogens. With the desire to guide the contraction of fibers in a controlled manner, the effect of alignment of mesogens on the contraction rate was discussed (Figure 2a). In the absence of an applied load, fibers with a stretching ratio of 100% only contracted 65% of their original lengths. When the fiber was stretched to 400%, the contraction rate reached up to 81% and remained unchanged with the increase of the stretching ratio. According to 2D XRD experiments, the order parameter of the fiber with a stretching ratio of 100% was calculated as about 0.47, while the value at a stretching ratio of 400% was nearly 0.69 similar to that of a fiber with the stretching ratio of 900% (Figure S9 and S10, Supporting Information). These observations confirm that the alignment of mesogens indeed influences the contraction

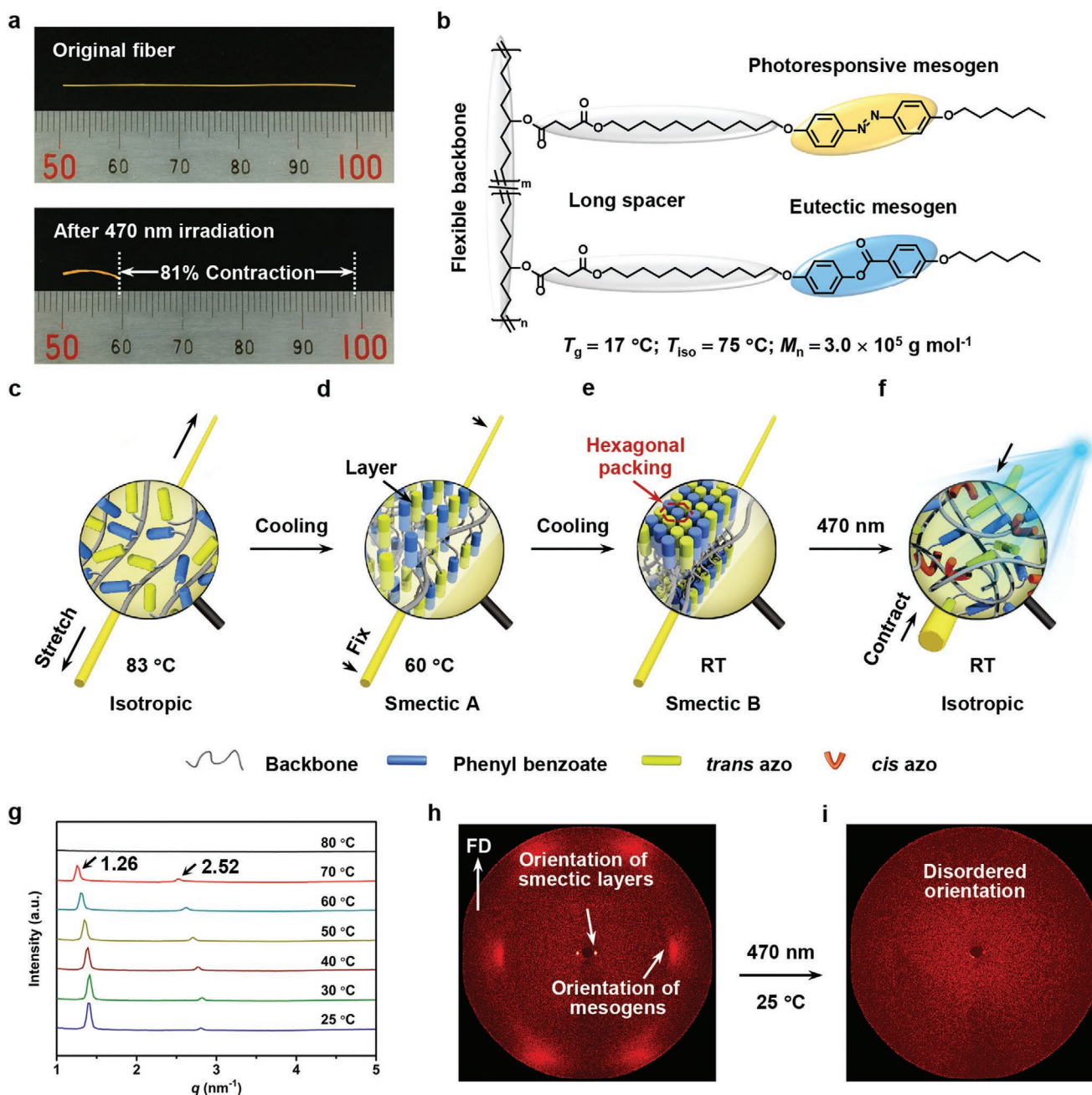


Figure 1. a) Photographs showing light-driven contraction up to 81% of the LLCPC fiber upon irradiation with 470 nm light (100 mW cm^{-2}). b) Molecular structure of a newly designed LLCPC. T_g , glass transition temperature; T_{iso} , isotropic transition temperature; M_n , number-average molecular weight. c–f) Schematics showing the fabrication procedure of the LLCPC fiber with highly ordered liquid crystal phase and mechanism of the light-driven ultralarge contraction based on *trans*–*cis* isomerization of azobenzene mesogens. RT, room temperature. g) A set of 1D SAXS profiles of the LLCPC fiber recorded upon cooling at different temperatures after stretched to 900%. The q ratio of 1:2 for the two low-angle diffractions indicates the formation of lamellar structures. The layer thickness is 4.98 nm at 70 °C. h, i) 2D XRD patterns recorded of a LLCPC fiber at the original state and after 470 nm light irradiation for 10 s at room temperature, respectively. The X-ray beam is perpendicular to the fiber direction. The light intensity is 100 mW cm^{-2} .

rate. Several representative reports of contraction of LCPs are summarized in Figure 2b.^[5c,e,f,h–k,6a,b] As illustrated, most of the thermal-driven contraction rates of LCPs were below 50%, and the contractions induced by photochemical effect only reached a largest rate of 20%. The contraction rate achieved in our work is four times larger than the reported light-driven contractions.

Such ultralarge contraction is attributed to several points: 1) the highly ordered SmB as the switching segment is a prerequisite for achieving large contraction rate, which constrains the backbones at room temperature and ensures that the strain energy is locked in the fibers; 2) the stretching is an essential step for the fibers to form the SmB phase with high-order parameters. Figure 2a has demonstrated that a fiber with the

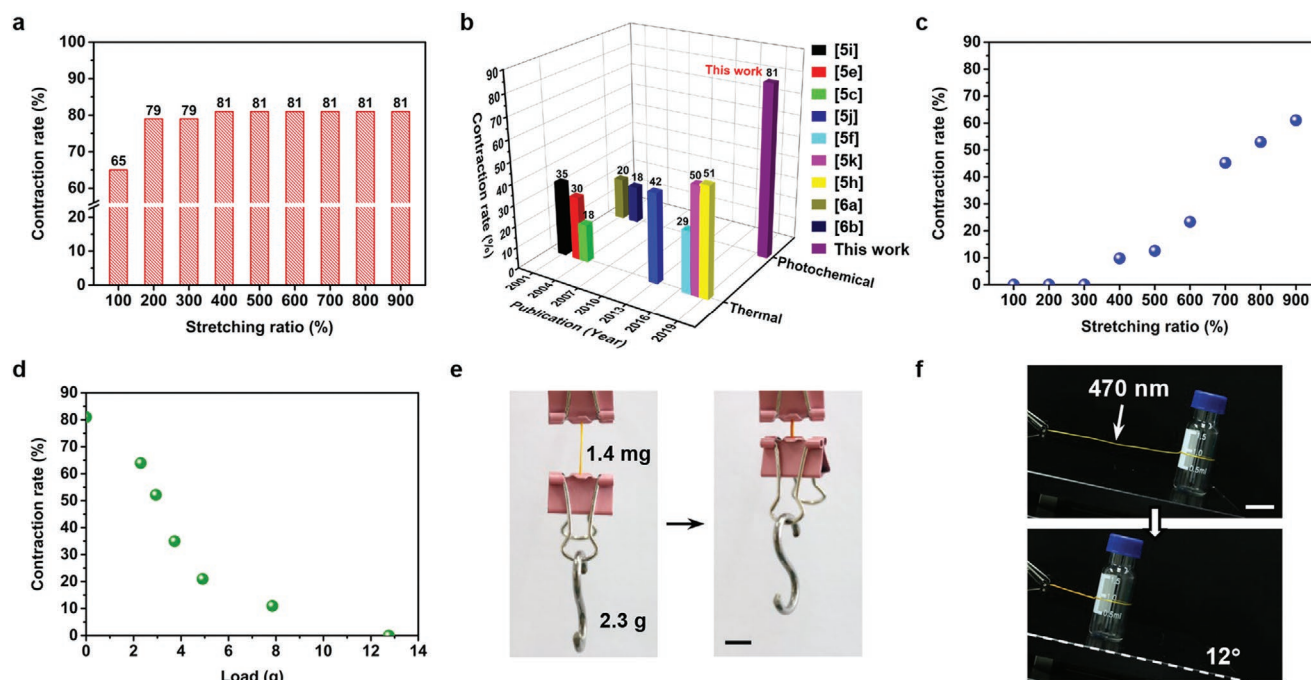


Figure 2. a) Light-driven contraction rates versus stretching ratios of the LLCPC fibers. b) Comparative summary of contraction rates in previous representative reports and this work. The contraction rate is defined as $f = ((l_0 - l')/l_0) \times 100\%$, where l_0 is the original length of the material and l' is the length after complete contraction. c) Influence of different stretching ratios on contraction rates of the LLCPC fibers lifting up a load (2.6 g). d) A plot showing contraction rates of the LLCPC fibers in a uniform size lifting up different loads. The stretching ratio of these fibers is 900%. e) Photographs showing a LLCPC fiber lifting up a counterpoise and a clamp (2.3 g in total) upon irradiation with 470 nm light, which are 1640 times heavier than its own weight. f) Lateral photographs showing a LLCPC fiber dragging a glass bottle (2.6 g) uphill on a 12° incline upon irradiation with 470 nm light. Scale bar: 1 cm. The light intensity is 100 mW cm⁻². The diameter of all the fibers used in experiments is 350 μm.

stretching ratio of 400% already possesses a highly ordered structure to achieve the contraction rate of 81%. In contrast, an unstretched LLCPC strip exhibits a disordered state after annealing (Figure S11, Supporting Information); 3) the large degree of change in the LC order plays a critical role in the achievement of large contraction rate. As shown in Figure S10 (Supporting Information), a LLCPC fiber (the stretching ratio is 900%) with a high order parameter of 0.70 became completely disordered upon light irradiation; 4) a plausible theory has been proposed that *trans-cis-trans* cycles of azobenzenes give rise to the decrease of T_g and drive polymers to “flow.”^[14] We assume that this phenomenon has also occurred here and the reduction of T_g further facilitates the movement of polymer segments. Moreover, the *trans-cis-trans* oscillation of azobenzene mesogens plays an important role in the creation of free volume, leading to an enhanced chain mobility.^[14,15] Recently, Zhao and co-workers have also demonstrated crosslinked LCP films with uniaxial alignment by stretching and fixed the stretched film using transesterification reaction. However, they paid more attention to the light-driven mechanical force upon both photothermal and photochemical effects rather than large contraction deformation.^[16]

In engineering applications, actuating materials must both bear loads and change shapes.^[5b] The influence of the stretching ratio on the fiber bearing loads was also investigated (Figure 2c). The contraction rate increases linearly with the stretching ratio, which can be related to a larger fiber strain that results in a greater force to counter the gravity force of the

load, since the polymer chain relaxation plays a primordial role in the contraction.^[16] Moreover, the heavy-lifting capability of the fibers with the stretching ratio of 900% was performed by adding different weights at their ends, which demonstrates a clear trend that the heavier the load is imposed, the smaller the contraction rate is (Figure 2d; Figure S12, Supporting Information).^[17] As shown in Figure 2e, one single fiber contracted 64% of its original length and lifted up a load of 2.3 g in total, which was 1640 times heavier than the fiber’s own weight (Movie S1, Supporting Information). The work capacity of this fiber actuator was calculated as about 80.8 kJ m⁻³ ($g = 9.803 \text{ m s}^{-2}$), which was two times higher than the average value of skeletal muscles (40 kJ m⁻³).^[5b,d] The isostrain measurement carried out at room temperature suggests that the fiber with the stretching ratio of 900% generates a contractile force reaching up to 2.2 MPa upon irradiation with 470 nm light (Figure S13, Supporting Information). Furthermore, the fiber was also capable of dragging a glass bottle which was nearly 1260 times heavier than its own weight uphill on a 12° incline, by contracting 65% of the original length (Figure 2f). It should be emphasized that the Young’s modulus of fibers remained almost unchanged during contraction due to the fibers were in a *trans*-rich state upon irradiation with 470 nm light. If the stimulus is switched to 365 nm UV light, the fibers will reach a *cis*-rich state and cannot bear heavy loads due to the significant decrease in the Young’s modulus.^[18]

Encouraged by the ultralarge contraction of the LLCPC fibers, we demonstrated the precise folding of a prototype foldout. The

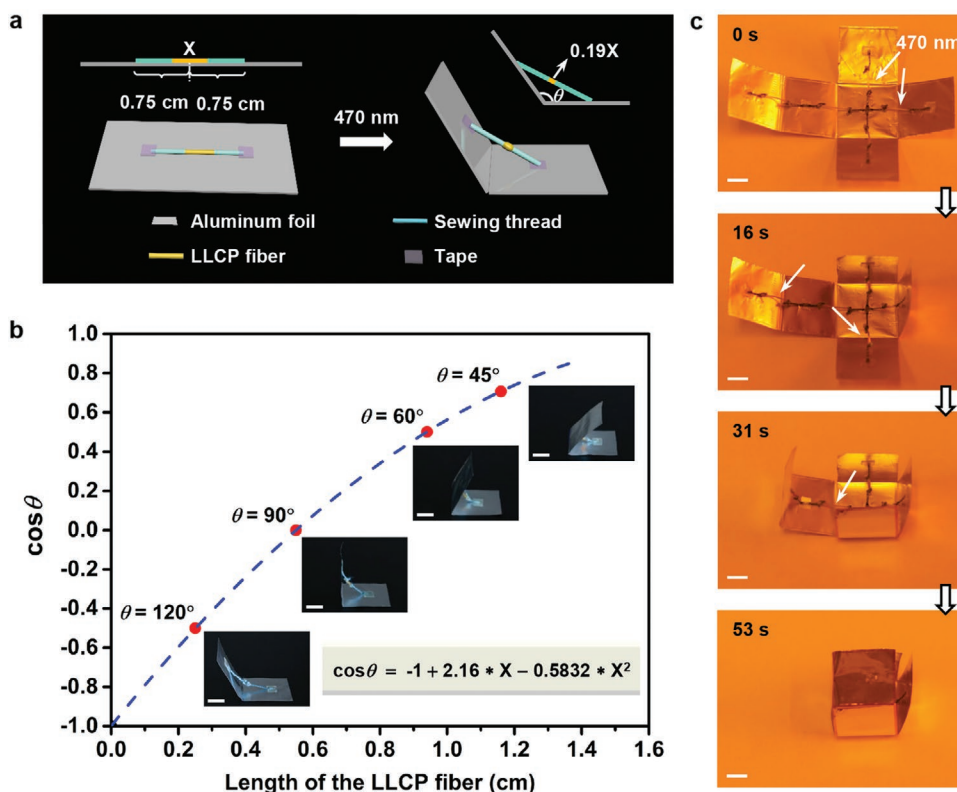


Figure 3. Light-driven precise origami. a) Schematics showing the light-driven folding of a prototype foldout. The hinge consists of two inactive sewing threads and a light-driven LLCF fiber. b) A plot of the folding angle as a function of the length (X) of the LLCF fiber. Inset photographs show the experimental results in prototype foldouts with different folding angles determined by the length of the LLCF fiber. Dashed line, curve of the inset equation. c) Photographs showing the programmed and precise folding of a box upon irradiation with 470 nm light according to the prototype foldout with the folding angle at 90° . The origami pattern consists of five 1.5 cm hinges containing a 0.55 cm LLCF fiber. The white arrows indicate the position of irradiation. The light intensity is 100 mW cm^{-2} . Scale bar: 5 mm.

foldout contained two parts, a passive substrate composed of two aluminum foil squares, and a hinge with a heterogeneous structure including two inactive sewing threads and a light-driven LLCF fiber (Figure 3a). Instead of inserting the active hinge at the crease by using ink printing method,^[19] we here affixed both ends of the hinge on the center of two adjacent facets, respectively. The combined length of the LLCF fiber and the sewing thread was defined as 1.5 cm, which was the same length as the sides of the aluminum foil square. Upon irradiation with 470 nm light, the LLCF fiber contracted up to 81% of its original length but the sewing thread remained unchanged, resulting in a shortening of the entire hinge and the folding of the aluminum foil.

Since the maximum contraction rate of the LLCF fiber is fixed at 81%, the folding angle θ can therefore be expressed by

$$\cos \theta = -1 + 2.16 \times X - 0.5832 \times X^2 \quad (1)$$

Equation (1) plotted as the dashed curve in Figure 3b represents a master curve for folding of the foldout for any angle within 0° to 180° . We measured the folding angle of foils with different lengths of fibers. The experimental data are shown in solid circle symbols, representing the cases in which complete folding is observed. It clearly shows that the measured results agree extremely well with the model prediction. Using

this mathematical model to predict the folding process, we demonstrated the programmed and precise folding of a box upon irradiation with 470 nm light with the folding angle at 90° (Figure 3c; Movie S2, Supporting Information). Recently, White and co-workers reported the all-optical closing of a box by using a 90° twisted nematic topological pattern to circumvent anti-clastic curvature at the facet/hinge interfaces, but could not control the folding angle.^[20] In our work, the folding angle was precisely controlled through the ingenious design of the hinge, which enabled the high fidelity of the target shape. Based on the simplicity and accuracy of this method, we believe that it will provide key momentum for the advance of precise origami.

For material scientists and engineers, nature provides endless sources of inspiration. Spider webs, for instance, have the ability to recover to the original state after being impacted by prey due to their supercontractility.^[21] Inspired by this phenomenon, we demonstrated the recovery of a “broken” spider web upon irradiation with 470 nm light (Figure 4a). By controlling the contraction rate to 81%, the loose spiral threads that were made of the LLCF fibers recovered to the original length of the intact spider web. Except for the recovery of the spider web, we also showed the light-driven closing of a string bag, in which two 26 mm plastic balls were held due to the contraction of the LLCF fiber (Figure 4b). Furthermore, a catching net with the mesh of $7 \text{ mm} \times 7 \text{ mm}$ was fabricated by weaving twisted fibers

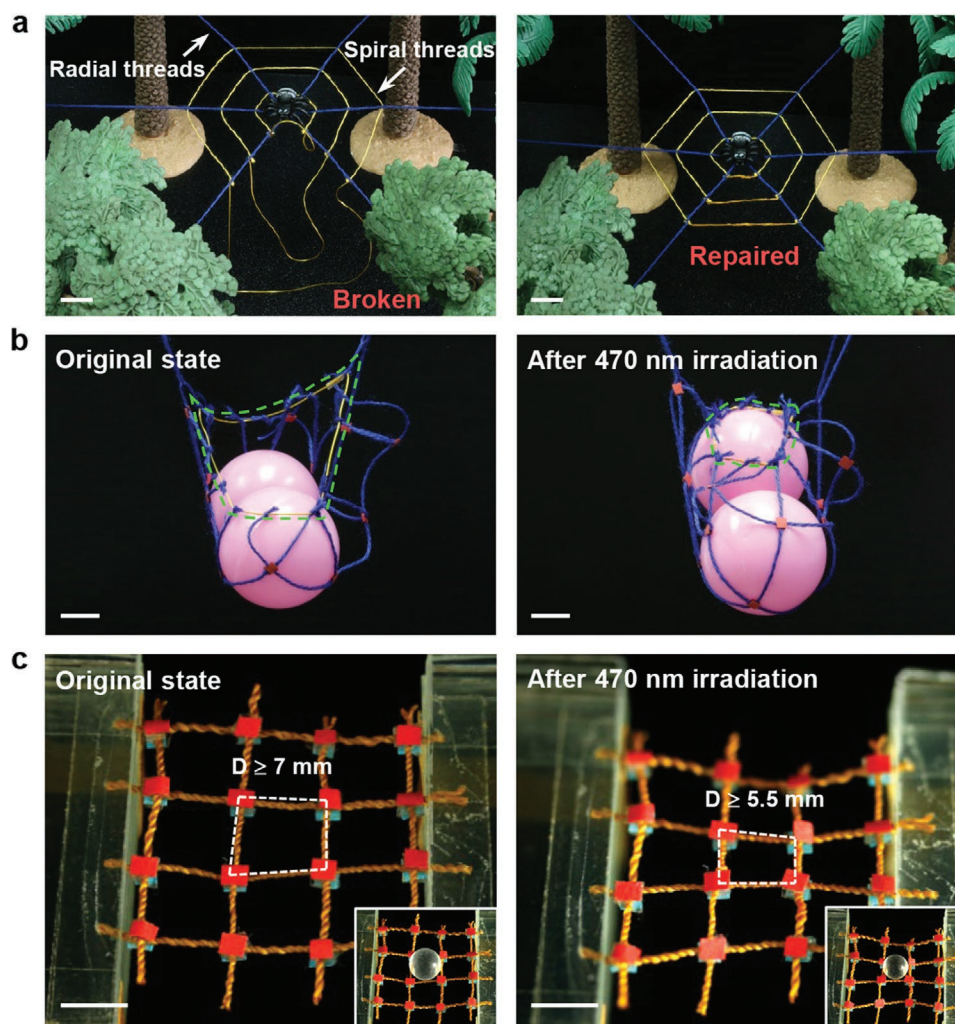


Figure 4. a) The recovery of a “broken” spider web upon irradiation with 470 nm light. The loose spiral threads are made of the LLCPC fibers that recover to the original length of the intact spider web by light-driven 81% contraction. Scale bar: 1 cm. b) Demonstration of light-driven closing of a string bag by using the LLCPC fiber. The dashed green line indicates the position of the fiber. Scale bar: 1 cm. c) Photographs showing a catching net woven from twisted fibers to screen glass balls in different sizes upon irradiation with 470 nm light. Inset: a 7 mm (left) and a 5.5 mm glass ball (right) are caught by the net before and after light irradiation, respectively. Scale bar: 5 mm. The light intensity in all these experiments is 100 mW cm^{-2} .

enabling improved strength for actuators (Figure 4c; Figure S14, Supporting Information). Upon irradiation with 470 nm light, the contraction of twisted fibers allowed the net to screen glass balls in diameters greater than or equal to 5.5 mm (Movie S3 and Figure S15, Supporting Information). To recycle the actuators, the contracted fibers can be reheated to the temperature higher than T_{iso} and stretched to fabricate new fibers, which exhibit the light-driven contraction rather similar to the initially prepared fibers (Figure S16, Supporting Information).

3. Conclusion

In conclusion, we have developed a conceptually novel strategy to realize the light-driven contraction in the LLCPCs based on the storage and release of the strain energy (inspired by SME), and demonstrated the ultralarge contraction up to 81% in the LLCPC fibers. It is worth mentioning that post-tension annealing

is critical for the LLCPC fibers to self-assemble into the highly ordered SmB phase, which serves as the switching segment for locking the strain energy in high-elastic fibers. The strain energy is unlocked because of the order–disorder phase transition upon reversible *trans–cis* isomerization of azobenzene mesogens by using 470 nm light as a “key.” The incorporation of phenyl benzoate groups as the eutectic mesogens, which largely activates the chain mobility by reducing the T_g below room temperature, is also beneficial for the release of the strain energy. Furthermore, the LLCPC fibers were used as light-driven hinges for precise origami and as silks for imitating the recovery of broken spider webs. Moreover, two kinds of nets woven from the fibers realized the holding and screening objects in different sizes. We believe that the strategy will facilitate the development of future investigations on light-driven large deformation of the LCPs, and also advance new applications of the LLCPCs in soft robotics, muscle-like actuators, and smart textiles.

4. Experimental Section

Materials: All the reagents were purchased from Adamas-beta, J&K Scientific, and Sigma Aldrich, and were used as received unless otherwise noted. Dichloromethane was purified by distillation over CaH₂. Synthesis and characterization of the LLCPS are described in the Supporting Information.

Preparation of the LLCPS Fibers: The LLCPS was first heated to the isotropic phase (83 °C) and held for 10 s to equilibrate the system, and shaped into a rod-like form. The melted polymer rod was uniaxially stretched to different elongations quickly by using two forceps. Then both ends of the fiber were fixed and cooled down to room temperature. After holding for 24 h, the clips used to fix both ends of the fiber were removed, and the fiber remained the fixed shape without a rebound.

Measurements: ¹H NMR spectra were recorded on a Bruker AVANCE III spectrometer (400 MHz) at room temperature using CDCl₃ as the solvent. The molecular weights and polydispersity indexes were measured by the gel permeation chromatography (GPC, SHIMADZU, LC-10ADvp) using THF as the mobile phase. Differential scanning calorimetry (DSC) measurement was performed using TA Q2000 analyzer operated at a scanning rate of 10 °C min⁻¹ under nitrogen atmosphere. Textures of the LLCPS were observed on a polarizing optical microscope (POM, Leica DM2500P) equipped with a Mettler hot stage (models FP-90 and FP-82). The 2D XRD pattern of the LLCPS fiber at room temperature shown in Figure 1h was obtained according to the previously reported literature.^[14] The 2D XRD experiment on the LLCPS fiber at 60 °C was conducted on a Ganesha system (SAXSLAB, USA) equipped with a multilayer focused Cu K α radiation as the X-ray source (Genix3D Cu ULD) and a 2D semiconductor detector (Pilatus 100 K, DECTRIS, Swiss). The scattering peak positions were calibrated with LaB₆ for high-angle region. A Linkam HFSX350-GI stage was used to investigate the structure evolution as a function of temperature. Both ends of the fiber were fixed with clamps during testing. The tensile stress-strain and isostrain measurements of the LLCPS fibers were performed on an Instron Testing Machine (Model 5943) at room temperature. By applying 470 nm light (normal incidence, light source 5 cm away) to a LLCPS fiber (5 mm \times 350 μ m, the stretching ratio is 900%) held under constant strain (within 0.2%), the contractile force generated in the fiber can be sensed and measured. Photographs and movies of light-driven contractions were recorded by a camera (Canon 70D) equipped with a filter to remove light with wavelengths below 530 nm. 470 nm visible light was generated by an LASEVER light source with an LSR-PS-II laser power supply.

Supporting Information

Supporting Information is available from the Wiley Online Library or from the author.

Acknowledgements

This work was financially supported by the National Natural Science Foundation of China (Grant Nos. 21734003, 51927805, 51721002) and Innovation Program of Shanghai Municipal Education Commission (2017-01-07-00-07-E00027).

Conflict of Interest

The authors declare no conflict of interest.

Keywords

fibers, light-driven contraction, liquid crystal polymers, phase transition, strain energy

Received: March 16, 2020
Revised: April 28, 2020
Published online: July 1, 2020

- [1] a) I. Agnarsson, A. Dhinojwala, V. Sahni, T. A. Blackledge, *J. Exp. Biol.* **2009**, *212*, 1990; b) T. A. Blackledge, C. Boutry, S. C. Wong, A. Baji, A. Dhinojwala, V. Sahni, I. Agnarsson, *J. Exp. Biol.* **2009**, *212*, 1981; c) C. Boutry, T. A. Blackledge, *J. Exp. Biol.* **2010**, *213*, 3505; d) H. Kim, Y. Jang, D. Y. Lee, J. H. Moon, J. G. Choi, G. M. Spinks, S. Gambhir, D. L. Officer, G. G. Wallace, S. J. Kim, *ACS Appl. Mater. Interfaces* **2019**, *11*, 31162.
- [2] S. M. Mirvakili, I. W. Hunter, *Adv. Mater.* **2018**, *30*, 1704407.
- [3] a) C. S. Haines, M. D. Lima, N. Li, G. M. Spinks, J. Foroughi, J. D. W. Madden, S. H. Kim, S. L. Fang, M. J. de Andrade, F. Goktepe, O. Goktepe, S. M. Mirvakili, S. Naficy, X. Lepro, J. Y. Oh, M. E. Kozlov, S. J. Kim, X. R. Xu, B. J. Swedlove, G. G. Wallace, R. H. Baughman, *Science* **2014**, *343*, 868; b) A. Toncheva, F. Khelifa, Y. Paint, M. Voué, P. Lambert, P. Dubois, J.-M. Raquez, *ACS Appl. Mater. Interfaces* **2018**, *10*, 29933; c) Y. Wu, D. U. Shah, B. Wang, J. Liu, X. Ren, M. H. Ramage, O. A. Scherman, *Adv. Mater.* **2018**, *30*, 1707169.
- [4] a) L. Montero de Espinosa, W. Meesorn, D. Moatsou, C. Weder, *Chem. Rev.* **2017**, *117*, 12851; b) Q. Li, *Photoactive Functional Soft Materials: Preparation, Properties and Applications*, Wiley-VCH, Weinheim, Germany **2019**; c) H. K. Bisoyi, Q. Li, *Chem. Rev.* **2016**, *116*, 15089; d) M. Yang, Z. Yuan, J. Liu, Z. Fang, L. Fang, D. Yu, Q. Li, *Adv. Opt. Mater.* **2019**, *7*, 1900069.
- [5] a) S. V. Ahir, A. R. Tajbakhsh, E. M. Terentjev, *Adv. Funct. Mater.* **2006**, *16*, 556; b) H. Kim, J. M. Boothby, S. Ramachandran, C. D. Lee, T. H. Ware, *Macromolecules* **2017**, *50*, 4267; c) M.-H. Li, P. Keller, J. Yang, P.-A. Albouy, *Adv. Mater.* **2004**, *16*, 1922; d) H.-F. Lu, M. Wang, X.-M. Chen, B.-P. Lin, H. Yang, *J. Am. Chem. Soc.* **2019**, *141*, 14364; e) J. Naciri, A. Srinivasan, H. Jeon, N. Nikolov, P. Keller, B. R. Ratna, *Macromolecules* **2003**, *36*, 8499; f) S. Nocentini, D. Martella, D. S. Wiersma, C. Parmeggiani, *Soft Matter* **2017**, *13*, 8590; g) C. Ohm, M. Morys, F. R. Forst, L. Braun, A. Eremin, C. Serra, R. Stannarius, R. Zentel, *Soft Matter* **2011**, *7*, 3730; h) D. J. Roach, C. Yuan, X. Kuang, V. C. F. Li, P. Blake, M. L. Romero, I. Hammel, K. Yu, H. J. Qi, *ACS Appl. Mater. Interfaces* **2019**, *11*, 19514; i) D. L. Thomsen, P. Keller, J. Naciri, R. Pink, H. Jeon, D. Shenoy, B. R. Ratna, *Macromolecules* **2001**, *34*, 5868; j) H. Yang, M.-X. Liu, Y.-W. Yao, P.-Y. Tao, B.-P. Lin, P. Keller, X.-Q. Zhang, Y. Sun, L.-X. Guo, *Macromolecules* **2013**, *46*, 3406; k) L. Yu, H. Shahsavani, G. Rivers, C. Zhang, P. Si, B. Zhao, *Adv. Funct. Mater.* **2018**, *28*, 1802809; l) X. Lu, H. Zhang, G. Fei, B. Yu, X. Tong, H. Xia, Y. Zhao, *Adv. Mater.* **2018**, *30*, 1706597; m) Y. Wu, Y. Yang, Q. Chen, X. Qian, Y. Wei, Y. Ji, *Angew. Chem., Int. Ed.* **2020**, *59*, 4778; n) L. Liu, M.-H. Liu, L.-L. Deng, B.-P. Lin, H. Yang, *J. Am. Chem. Soc.* **2017**, *139*, 11333; o) Z.-C. Jiang, Y.-Y. Xiao, L. Y. L. H. Y. Z. *Angew. Chem.* **2020**, *132*, 4955.
- [6] a) H. Finkelmann, E. Nishikawa, G. G. Pereira, M. Warner, *Phys. Rev. Lett.* **2001**, *87*, 015501; b) M.-H. Li, P. Keller, B. Li, X. Wang, M. Brunet, *Adv. Mater.* **2003**, *15*, 569.
- [7] a) X. Pang, J. A. Lv, C. Zhu, L. Qin, Y. Yu, *Adv. Mater.* **2019**, *31*, 1904224; b) X. Qing, J. A. Lv, Y. Yu, *Acta Polym. Sin.* **2017**, *11*, 1679; c) T. Ube, T. Ikeda, *Adv. Opt. Mater.* **2019**, *7*, 1900380.
- [8] T. Ikeda, J.-I. Mamiya, Y. Yu, *Angew. Chem., Int. Ed.* **2007**, *46*, 506.
- [9] a) T. Xie, *Nature* **2010**, *464*, 267; b) Q. Zhao, H. J. Qi, T. Xie, *Prog. Polym. Sci.* **2015**, *49*, 79.
- [10] a) C. Liu, H. Qin, P. T. Mather, *J. Mater. Chem.* **2007**, *17*, 1543; b) T. Xie, *Polymer* **2011**, *52*, 4985; c) J. Lai, X. Li, R. Wu, J. Deng, Y. Pan, Z. Zheng, X. Ding, *Soft Matter* **2018**, *14*, 7302.
- [11] a) J. A. Lv, Y. Liu, J. Wei, E. Chen, L. Qin, Y. Yu, *Nature* **2016**, *537*, 179; b) B. Xu, C. Zhu, L. Qin, J. Wei, Y. Yu, *Small* **2019**, *15*, 1901847; c) Q. Liu, Y. Yu, J. A. Lv, E. Chen, Y. Yu, *Adv. Intell. Syst.* **2019**, *1*, 190060; d) S.-Q. Han, Y.-Y. Chen, B. Xu, J. Wei, Y.-L. Yu, *Chin. J. Polym. Sci.* **2020**, <https://doi.org/10.1007/s10118-020-2383-0>.

- [12] a) T. Ikeda, S. Horiuchi, D. B. Karanjit, S. Kurihara, S. Tazuke, *Macromolecules* **1990**, 23, 42; b) O. V. Potemkina, S. A. Kuvshinova, O. I. Koifman, *Russ. J. Gen. Chem.* **2019**, 89, 597.
- [13] H.-L. Xie, C.-K. Jie, Z.-Q. Yu, X.-B. Liu, H.-L. Zhang, Z. Shen, E.-Q. Chen, Q.-F. Zhou, *J. Am. Chem. Soc.* **2010**, 132, 8071.
- [14] P. Weis, W. Tian, S. Wu, *Chem. - Eur. J.* **2018**, 24, 6494.
- [15] a) P. Weis, S. Wu, *Macromol. Rapid Commun.* **2018**, 39, 1700220; b) W.-C. Xu, S. Sun, S. Wu, *Angew. Chem., Int. Ed.* **2019**, 58, 9712; c) D. Liu, D. J. Broer, *Nat. Commun.* **2015**, 6, 8334; d) K. G. Yager, O. M. Tanchak, C. Godbout, H. Fritzsche, C. J. Barrett, *Macromolecules* **2006**, 39, 9311.
- [16] X. Lu, S. Guo, X. Tong, H. Xia, Y. Zhao, *Adv. Mater.* **2017**, 29, 1606467.
- [17] a) L. Jin, Z. Zeng, Y. Huo, *J. Mech. Phys. Solids* **2010**, 58, 1907; b) W. Kaufhold, H. Finkelmann, H. R. Brand, *Makromol. Chem.* **1991**, 192, 2555; c) J. Schätzle, W. Kaufhold, H. Finkelmann, *Makromol. Chem.* **1989**, 190, 3269.
- [18] a) H. Zhou, C. Xue, P. Weis, Y. Suzuki, S. Huang, K. Koynov, G. K. Auernhammer, R. Berger, H.-J. Butt, S. Wu, *Nat. Chem.* **2017**, 9, 145; b) X. Zhang, C. Zhu, B. Xu, L. Qin, J. Wei, Y. Yu, *ACS Appl. Mater. Interfaces* **2019**, 11, 46212.
- [19] Y. Liu, B. Shaw, M. D. Dickey, J. Genzer, *Sci. Adv.* **2017**, 3, e1602417.
- [20] B. R. Donovan, V. M. Matavulj, S.-K. Ahn, T. Guin, T. J. White, *Adv. Mater.* **2019**, 31, 1805750.
- [21] a) T. A. Blackledge, N. Scharff, J. A. Coddington, T. Szuts, J. W. Wenzel, C. Y. Hayashi, I. Agnarsson, *Proc. Natl. Acad. Sci. USA* **2009**, 106, 5229; b) S. W. Cranford, A. Tarakanova, N. M. Pugno, M. J. Buehler, *Nature* **2012**, 482, 72; c) C. C. F. Grannemann, M. Meyer, M. Reinhardt, M. J. Ramirez, M. E. Herberstein, A. C. Joel, *Sci. Rep.* **2019**, 9, 17273; d) F. G. Omenetto, D. L. Kaplan, *Science* **2010**, 329, 528.